crystals

Article

Cumulative Damage in Very High/Low Cycle Combined Fatigue for TC21 Titanium Alloy

Baohua Nie [1,2], Shuai Liu [1], Yue Wu [1], Yu Song [1], Haiying Qi [1,2], Binqing Shi [1,2], Zihua Zhao [3,*] and Dongchu Chen [1,2,*]

1 School of Materials Science and Hydrogen Energy, Foshan University, Foshan 528000, China
2 Guangdong Key Laboratory for Hydrogen Energy Technologies, Foshan 528000, China
3 School of Materials Science and Engineering, Beihang University, Beijing 100191, China
* Correspondence: zhzh@buaa.edu.cn (Z.Z.); chendc@fosu.edu.cn (D.C.); Tel.: +86-010-8233-3264 (Z.Z.); +86-075-7827-00525 (D.C.)

Abstract: The effect of low cycle fatigue (LCF) predamage with no precracks on very high cycle fatigue (VHCF) properties, and crack initiation characteristics for TC21 titanium alloy, was investigated. The results showed that LCF predamage with less than 5% of fatigue life had little influence on fatigue limit, but reduced its fatigue life. Fatigue cracks were initiated on the surface of the specimen at high stress amplitude, whereas fatigue cracks were initiated on the subsurface of the specimens at low stress amplitude. Based on Lemaitre damage theory, a very high/low cycle combined fatigue damage model was established to analyze the fatigue damage process, which was consistent with the experimental data. It was indicated that 5% LCF predamage value was the equivalent damage value, which was close to the critical value of VHCF crack initiation. The fatigue crack initiation of the specimens with LCF predamage less than 5% took up the major components of fatigue life.

Keywords: fatigue damage; VHCF; titanium alloy; combined fatigue

check for updates

Citation: Nie, B.; Liu, S.; Wu, Y.; Song, Y.; Qi, H.; Shi, B.; Zhao, Z.; Chen, D. Cumulative Damage in Very High/Low Cycle Combined Fatigue for TC21 Titanium Alloy. *Crystals* **2022**, *12*, 1702. https://doi.org/10.3390/cryst12121702

Academic Editor: Tomasz Sadowski

Received: 1 November 2022
Accepted: 19 November 2022
Published: 24 November 2022

1. Introduction

TC21 titanium alloy independently developed in China obtained high strength and toughness, and was widely used in key components of aviation structures [1]. In the process of aircraft service, key aviation components were subjected to low cycle fatigue (LCF) with low frequency and high stress, such as takeoff, landing, acceleration flight, etc. However, the key components of aviation underwent very high cycle fatigue (VHCF) with high frequency and low stress in ultra-long service life [2]. Under the coupling of high and low stress, very high/low cycle combined fatigue damage and life prediction played an important role in ensuring the high reliability service of key aviation components.

Research on the VHCF properties and fracture mechanism of titanium alloys mainly focused on the effect of microstructure [3], stress ratio [4], temperature [5,6] and other factors, but less effort was paid to VHCF/LCF combined fatigue. Huang et al. [7,8] showed that LCF predamage at 0.62% strain amplitude for 100 cycles significantly reduced the VHCF performance of A42 steel and promoted the initiation of multiple cracks on the surface of the specimen. In a previous study [9], LCF predamage at 950 MPa stress amplitude for 10% of its fatigue life formed precracks, reducing the VHCF limit of TC21 titanium alloy, where crack growth life took up the main part of fatigue life. LCF predamage with 5% of its fatigue life had no effect on the VHCF limit due to the absent of precracks, but reduced fatigue life. However, the effect of LCF damage with no precracks on the subsequent VHCF behavior was still not well understood.

As for high/low cycle combined fatigue damage, based on the fatigue nonlinear cumulative damage theory [10], some prediction models of combined fatigue life were developed considering the effect of the combined fatigue frequency ratio and stress amplitude ratio [11–13]. On the other hand, from the perspective of fatigue crack growth, when the stress intensity factors of superimposed high cycle fatigue load exceeded a certain critical threshold value, high cycle fatigue load promoted LCF crack growth [14]. The influence of LCF damage on the threshold value of HCF crack growth depended on stress ratio, crack depth and residual stress at crack tip [15]. Hu et al. [16] considered the influence of HCF stress ratio, and established a combined fatigue crack growth model based on crack closure effect. Moreover, deep learning [17] and probability statistics methods [18,19] had been used in the prediction of high/low cycle combined fatigue life in recent years. However, fatigue crack initiation was the main damage process for VHCF [20], and a continuous damage mechanical model needed to be established [21]. Based on the theory of continuous damage mechanics, Lemaitre [22] proposed a two-scale fatigue damage model to describe the LCF and high cycle fatigue damage of materials. The author established a LCF damage model of TC21 titanium alloy, and analyzed LCF damage evolution [23].

In this paper, the effect of LCF predamage with no precracks on VHCF properties and the crack initiation characteristics of TC21 titanium alloy was investigated. Based on Lemaitre damage theory, a VHCF/LCF combined fatigue damage model was established to analyze combined fatigue behavior and damage mechanism.

2. Experimental Procedures

2.1. Materials

TC21 titanium alloy with its nominal composition of Ti-6Al-2Zr-2Sn-2Mo- 2Nb-1.5Cr (wt.%) was used in this work. The alloys with basketweave microstructure obtained a tensile strength of 1070 MPa and a yield stress of 970 MPa, respectively [24].

2.2. VHCF/LCF Combined Fatigue Tests

VHCF tests were preferentially carried out by ultrasonic fatigue test machine (SHIMADZU, Kyoto, Japan) at a load ratio of R = −1, which was an accelerating testing method with 20 kHz frequency. Detailed introduction of equipment can be referred to the literature [25]. The specimen geometry was designed based on the elastic wave theory as the amplifier and the specimen must work at resonance. The geometries and dimensions of the fatigue specimens was illustrated in Figure 1. Thus, ultrasonic fatigue specimens were used for VHCF/LCF combined fatigue tests.

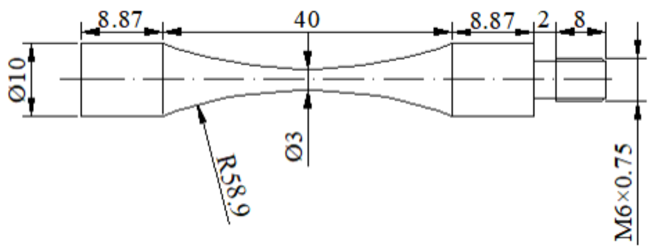

Figure 1. Geometries and dimensions of the test specimens.

Firstly, uniaxial stress controlled LCF of ultrasonic fatigue specimens were tested by using a conventional hydraulic fatigue machine (Instron 8801, Instron Company, Boston, MA, USA), and subsequent VHCF tests were performed by using ultrasonic fatigue test machine at different stress amplitude. Both LCF and VHCF tests were carried out at a load ratio of R = −1.

Based on the previous research [9], no LCF precracks can be formed at 950 MPa stress for cycles less than 90 cycles for TC21 titanium alloy. Thus, LCF predamage was applied at 950 MPa stress for 90 cycles (5% of fatigue life), 45 cycles (2.5% of fatigue life), 9 cycles (0.5% of fatigue life), respectively. LCF predamage was respectively abbreviated as 5% predamage, 2.5% predamage and 0.5% predamage in this paper.

The subsequent ultrasonic fatigue test was conducted at between 550 MPa and 430 MPa stress amplitude, where fatigue crack initiated on subsurface of TC21 titanium alloy in very high cycle regime [9].

The specimens underwent electro-polishing (EP) to remove the machining layers. Fatigue fracture was observed by scanning electron microscope (CS3400, Cambridgeshire, UK).

3. Results and Discussion

3.1. Effect of LCF Predamage on S-N Curves

Figure 2 shows 0.5 predamage had no significant effect on the fatigue properties of TC21 titanium alloy compared with that without predamage. Fatigue limit after less than 5% predamage was not decreased significantly, which can be attributed to the absent of precracks [9]. However, fatigue life decreased significantly with the increase in LCF predamage, as crack initiation life deceased by the activation of slip deformation at specimen surface due to LCF predamage [26]. Fatigue life of 5% predamage specimens at 470 MPa stress amplitude decreased by two orders of magnitude compared with that of undamaged specimens. The fatigue life of 2.5% predamage specimens was lower than that of undamage specimens, but higher than that of 5% predamage specimens.

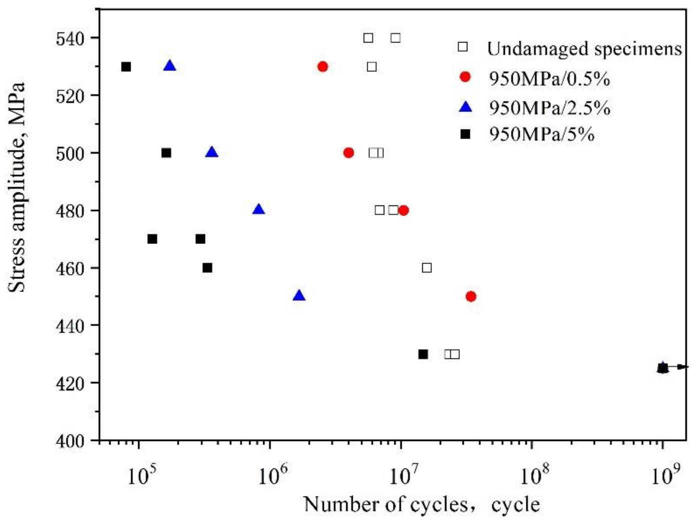

Figure 2. S-N curves of predamaged specimens for TC21 titanium alloy (arrows denote the run-out specimens).

3.2. Fracture Analysis

The fatigue fracture of TC21 titanium alloy after different predamage are shown in Figures 3–5. For the 0.5% predamage specimens, fatigue crack initiated inside the specimens, and the crack initiation site was characterized by the bright particles (Figure 3), which was consistent with VHCF crack initiation characteristics of the undamaged specimens [9]. For 2.5% predamage specimens, the crack initiated on the specimen surface at relatively high stress amplitude (Figure 4). Although no obvious fatigue precracks were observed, the resistance to surface fatigue crack initiation was weakened as the slip system of materials were activated by LCF plastic deformation [26]. However, fatigue cracks initiated on the subsurface of the specimens at a relatively low stress amplitude of 450 MPa, indicating that 2.5% predamage was not enough to promote the surface cracks initiation at a low stress amplitude. Moreover, the crack initiation area was typical bright particle feature (Figure 5), illustrating the same characteristics of fatigue crack initiation as undamaged specimens. The crack initiation characteristics of 5% predamage specimens were similar to that of 2.5% predamage, and the specific fracture morphology can refer to the previous research [9].

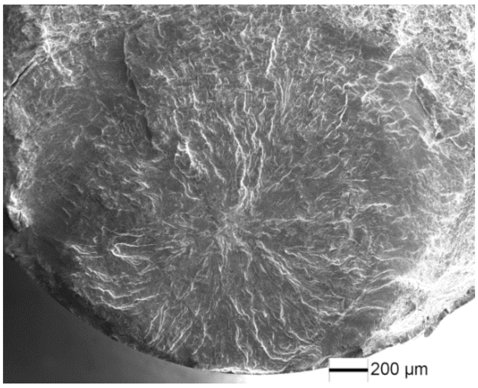

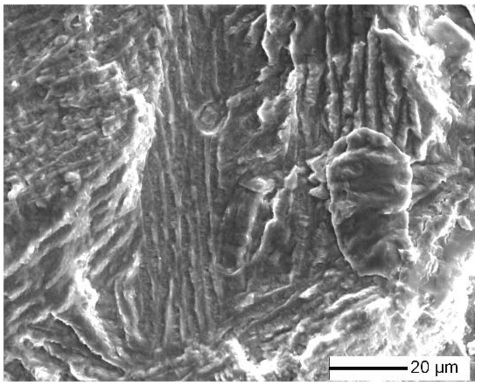

(**a**) (**b**)

Figure 3. Fracture surface for 0.5% predamage specimens at σ = 450 MPa and N = 3.44 × 10^7 cycles: (**a**) macroscopic morphology, and (**b**) crack initiation morphology.

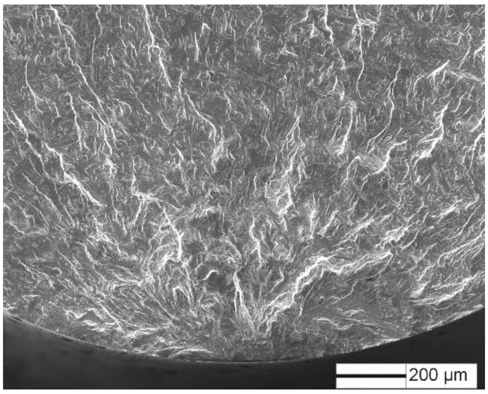

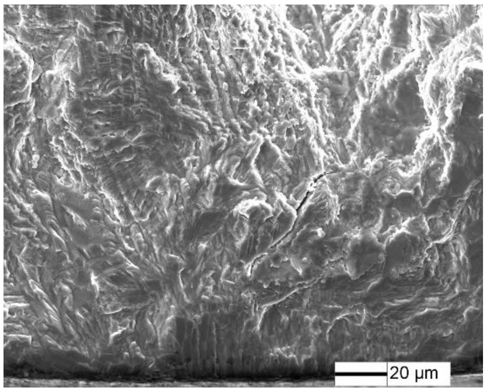

(**a**) (**b**)

Figure 4. Fracture surface for 2.5% predamage specimens at σ = 500 MPa and N = 3.4 × 10^5 cycles: (**a**) macroscopic morphology, and (**b**) crack initiation morphology.

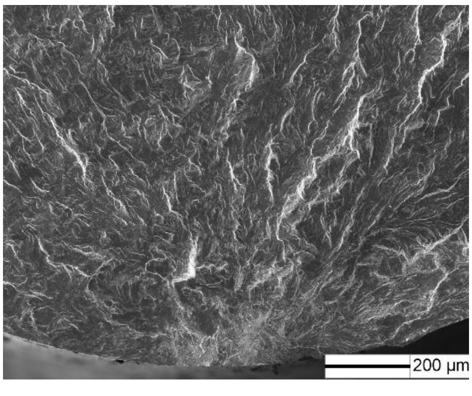

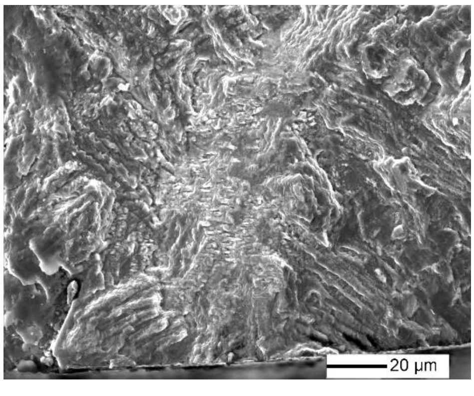

(**a**) (**b**)

Figure 5. Fracture surface for 2.5% predamage specimens at σ = 450 MPa and N = 1.8 × 10^6 cycles: (**a**) macroscopic morphology, and (**b**) crack initiation morphology.

3.3. Very High/Low Cycle Combined Fatigue Damage and Life Prediction

3.3.1. VHCF Damage Model

According to the two-scale fatigue damage model established by Lemaitre [22], the fatigue damage rate of VHCF at micro-scale can be expressed as:

$$\mathrm{d}D = \left[\frac{(\sigma_a + C\sigma_f)^2 R_\nu^\mu}{2ES(1+C)^2(1-D)^2} \right]^s \frac{\mathrm{d}\sigma_a}{k(1+C)} \tag{1}$$

where superscript μ represents micro variable. The damage strength S represented the amount of fatigue damage produced by each plastic strain increment. The parameter s represented the nonlinear cumulative parameter of fatigue damage. σ_a was stress amplitude, σ_f was VHCF limit. The parameters of C and k were material constant.

R_ν^μ was triaxial stress state function, and can be expressed as [22]:

$$R_\nu^\mu = \frac{2}{3}(1+\nu) + 3(1-2\nu)[\frac{(1+C)}{3(1+C\frac{\sigma_f}{\sigma_a})}]^2 \tag{2}$$

A stress cycle integral was performed for Equation (1), and fatigue damage of each cycle was [22]:

$$\frac{\delta D}{\delta N} = \frac{2(R_\nu^\mu)^s\left[(\sigma_a + C\sigma_f)^{2s+1} - [\sigma_f(1+C)]^{2s+1}\right]}{k(1+C)(2s+1)[2ES(1+C)^2(1-D)^2]^s} \tag{3}$$

For Equation (3), the value of fatigue damage D was integrated from 0 to D, and fatigue damage D for different cycles was calculated as:

$$D = 1 - [1 - \frac{2(R_\upsilon^\mu)^s[(\sigma_a + C\sigma_f)^{2s+1} - [\sigma_f(1+C)]^{2s+1}]}{(2ES)^s k(1+C)^{2s+1}} N]^{\frac{1}{2s+1}} \tag{4}$$

Fatigue crack initiated as fatigue damage D reached the critical damage value of fatigue crack initiation D_c, and its crack initiation life was:

$$N_R = [1-(1-D_c)^{(2s+1)}] \frac{(2ES)^s k}{2(R_\nu^\mu)^s[(\frac{\sigma_a + C\sigma_f}{1+C})^{2s+1} - {\sigma_f}^{2s+1}]} \tag{5}$$

For VHCF, crack initiation life accounted for a major proportion, while the crack propagation life accounted for a small one. If crack growth life was ignored, Formula (5) can be considered as the relationship between fatigue stress and life.

The parameters in Formula (5) are summarized in Table 1. Assuming that the hardening dynamics of the micro-scale was the same as that of the mesoscale, the parameter k was determined as 1067.3 MPa from the stress-strain curve [24]. The material parameter C can be calculated by the formula C = 3aE/2k, where the parameter a was taken as 0.4 [22]. For VHCF fracture (crack initiation), the critical damage value D_c was [27]:

$$D_C = D_{IC}(\frac{\sigma_u}{\sigma_f})^2 \tag{6}$$

where σ_u was the tensile strength of the material, and the critical damage of tensile fracture D_{IC} was generally taken as 0.1 [27].

Table 1. VHCF damage parameters of TC21 titanium alloy.

E (GPa)	σ_u (MPa)	σ_f (MPa)	k (MPa)	C	S (MPa)	B_0	Dc
110 [24]	1070 [24]	430 [9]	1067.3 [24]	61.84 calculation	130 [24]	1.64 fitting	0.62 calculation

The nonlinear fatigue damage parameter s was a function of stress amplitude σ_a. Referring to the Chaboche damage mechanics model [7], the nonlinear fatigue damage parameter s can be expressed as:

$$s = B_0 \left(\frac{\sigma_u - \sigma_a}{\sigma_u - \sigma_f} \right) \tag{7}$$

where B_0 was the adaptive parameter of the fatigue damage accumulation process. By fitting the S-N curve of the undamaged specimens (Figure 6), the parameter of B_0 was equal to 1.64 using the numerical iteration calculation.

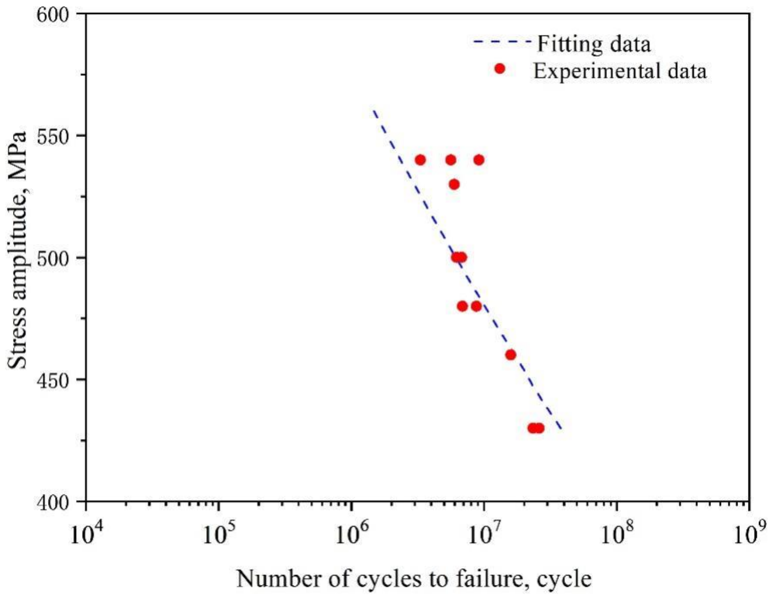

Figure 6. Fitting of fatigue damage parameters for TC21 titanium alloy.

Fatigue damage was usually evaluated by the reduction degree of elastic modulus of specimens [23]. However, VHCF damage had little effect on the elastic modulus of the specimen. It implied that there was almost no macroscopic fatigue damage for VHCF [7]. The investigation by Huang et al. [7] showed that the elastic modulus of ultrasonic fatigue specimens was linear with the resonant frequency, and ultrasonic fatigue damage can be characterized by the reduction of the specimen resonance frequency. In an ultrasonic fatigue test, the ultrasonic resonance frequency of specimens was designed between 19.5 and 20.5 kHz, and the initiation of fatigue cracks reduced the resonant frequency of the specimens. When the resonance frequency of the specimens was lower than 19.5 kHz, ultrasonic fatigue testing machine stopped working where fatigue crack initiated and propagated to fracture. Thus, VHCF cracks initiation corresponded to the reduction of the resonant frequency of the specimen by ($f_0 - 19.5$).

Considering the VHCF crack propagation life can be ignored, the VHCF damage model was based on the microscale damage of crack initiation; ultrasonic fatigue damage D_n can be characterized as:

$$D_n = \frac{f_0 - f_n}{f_0 - 19.5} \tag{8}$$

where f_0 was about 20 kHz due to the differences in specimens processing. f_n was the specimen resonance frequency at nth stress cycle which can be automatically monitored.

The resonant frequency of specimen at 450 MPa stress amplitude was measured to characterize fatigue damage, as shown in Figure 7. It indicated that fatigue damage based on this model was well agreed with the experimental data.

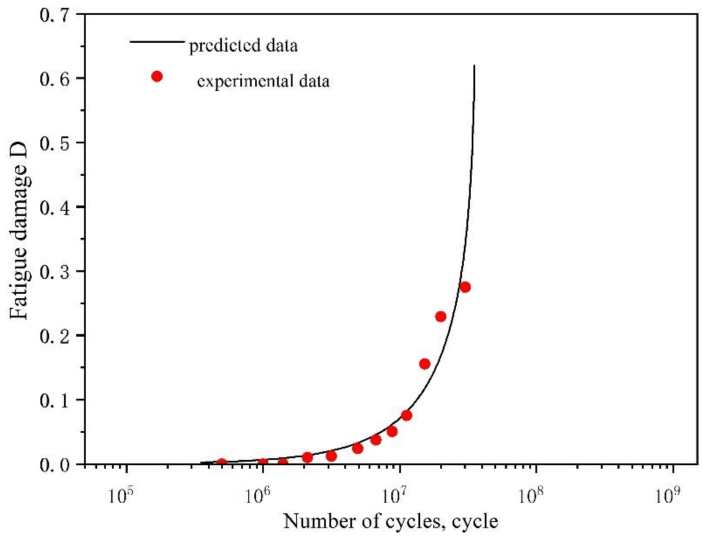

Figure 7. Comparison of the prediction of fatigue damage and experimental data at 450 MPa stress amplitude.

3.3.2. Prediction Model of Very High/Low Cycle Combined Fatigue

For very high/low cycle combined fatigue, it was necessary to consider the effect of LCF damage D_0 on the subsequent VHCF life. Integrated from the predamage D_0 to D by Equation (3), VHCF damage D value for different number of cycles was expressed as:

$$D = 1 - [(1 - D_0)^{(2s+1)} - \frac{2(R_v^\mu)^s[(\sigma_a + k\sigma_f)^{2s+1} - [\sigma_f(1+k)]^{2s+1}]}{(2ES)^s C(1+k)^{2s+1}} N]^{\frac{1}{2s+1}} \quad (9)$$

When D reached D_c, the crack initiation life can be calculated as:

$$N_R = [(1 - D_0)^{(2s+1)} - (1 - D_c)^{(2s+1)}] \frac{(2ES)^s C}{2(R_v^\mu)^s[(\frac{\sigma_a + k\sigma_f}{1+k})^{2s+1} - \sigma_f{}^{2s+1}]} \quad (10)$$

The detailed calculation process of LCF predamage D_0 at different cycles under 950MPa stress amplitude can refer to the previous study [23]. LCF predamage under 950 MPa stress amplitude for 5%, 2.5% and 5% of fatigue life was 0.000189, 0.000956 and 0.00193, respectively.

However, there was significant difference in fracture mechanisms between LCF and VHCF. LCF damage was mainly attributed to multiple crack propagation [24], and fatigue fracture can occur when fatigue damage reached to its critical damage. The VHCF damage was mainly caused by crack initiation, and fatigue cracks can initiate when fatigue damage reached to its critical damage. Therefore, the criterion of fatigue damage was different between LCF and VHCF. It was necessary to establish the conversion relationship between them when calculating very high/low cycle combined fatigue damage.

From the definition of damage, the damage value D can be expressed as:

$$D = \frac{A_D}{A} \quad (11)$$

where A_D was the area of damage, and A was the area of mesoscale.

The expression of the fatigue critical damage value D_c was:

$$D_c = \frac{A_c}{A} \tag{12}$$

where A_c was fatigue critical damage area.

According to Equations (11) and (12), LCF damage D_L and VHCF damage D_H can be expressed as:

$$D_L = (\frac{A_D}{A_{c,L}})D_{c,L} \tag{13}$$

$$D_H = (\frac{A_D}{A_{c,H}})D_{c,H} \tag{14}$$

where $A_{c,L}$ and $A_{c,H}$ were the critical damage areas of LCF and VHCF, respectively. $D_{c,H}$ can be calculated by Equation (6). $D_{c,L}$ were established as:

$$D_{c,L} = D_{IC}(\frac{\sigma_u}{\sigma_L})^2 \tag{15}$$

Based on the above fatigue damage model, the LCF critical damage area $A_{c,L}$ and the VHCF critical damage area $A_{c,H}$, respectively corresponded to the concepts of fatigue fracture toughness (K_{fr}) and fatigue crack growth threshold (ΔK_{th}). According to the stress intensity factor of surface crack [28], LCF fracture toughness was expressed as:

$$K_{fr} = 0.65\sigma_{\mathrm{a,L}}\sqrt{\pi\sqrt{A_{c,L}}} \tag{16}$$

As for the specimens with LCF predamage, the VHCF crack initiated near surface, and the fatigue crack growth threshold (ΔK_{th}) was given as:

$$\Delta K_{th} = 0.65\sigma_{\mathrm{a,H}}\sqrt{\pi\sqrt{A_{c,H}}} \tag{17}$$

According to Formulas (6), (13)–(17), the relationship between LCF damage D_L and VHCF damage D_H can be obtained as:

$$\frac{D_H}{D_L} = (\frac{K_{fr}}{\Delta K_{\mathrm{th}}})^4(\frac{\sigma_H}{\sigma_L})^4(\frac{\sigma_L}{\sigma_f})^2 = \alpha \tag{18}$$

Fatigue fracture toughness K_{fr} of TC21 titanium alloy was about 24 MPam$^{-1/2}$, which can be calculated from the reference [9], and ΔK_{th} was 2.78 MPam$^{-1/2}$ [9].

Therefore, LCF predamage $D_{0,L}$ can be converted into the equivalent VHCF damage value $\alpha D_{0,L}$, then VHCF initiation life N_H containing LCF predamage $D_{0,L}$ can be expressed as:

$$N_H = [(1-\alpha D_{0,L})^{(2s+1)} - (1-D_c)^{(2s+1)}]\frac{(2ES)^s C}{2(R_\nu^\mu)^s[(\frac{\sigma_a+k\sigma_f}{1+k})^{2s+1} - \sigma_f{}^{2s+1}]} \tag{19}$$

3.3.3. Prediction of Very High/Low Cycle Combined Fatigue Life

The calculation of very high/low cycle combined fatigue life for TC21 titanium alloy is shown in Figure 8. It indicats that fatigue life was reduced by varying degrees due to LCF predamage. The fatigue life of specimens with 0.5% predamage was similar to that without predamage, while the fatigue life of specimens with 5% predamage was significantly reduced. Moreover, the predicted data by this model was well agreed with the experimental data.

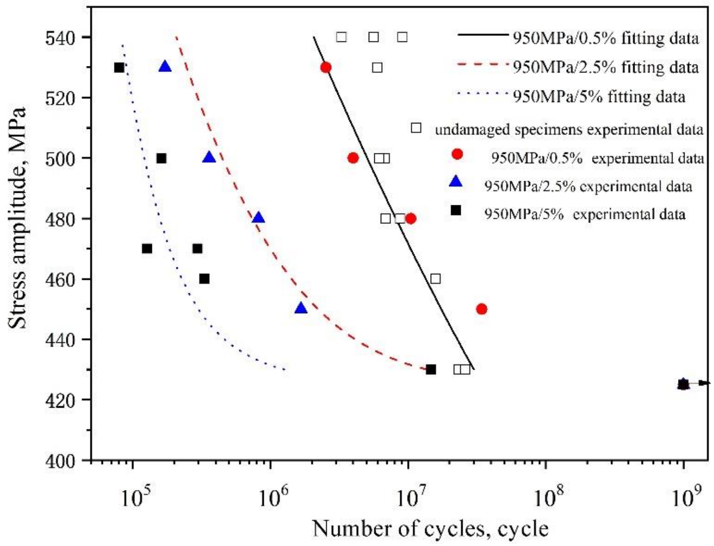

Figure 8. Fatigue life prediction of TC21 titanium alloy after LCF predamage.

Fatigue damage evolution for different LCF predamage specimens at 450 MPa stress amplitude is shown in Figure 9. The specimens with different LCF predamage illustrated a similar fatigue damage behavior. Fatigue damage significantly increased with the number of cycles, illustrating nonlinear damage characteristics. Based on the calculation of fatigue damage, 5% predamage value was equal to 0.00193, and the equivalent damage value was 0.54 for VHCF, which was close to the critical value of the VHCF crack initiation of TC21 titanium alloy. Fatigue cracks can easily initiate and propagate to fracture. Furthermore, fatigue life decreased with the increase of LCF predamage and stress amplitude (Figure 10). When the equivalent fatigue predamage reached 0.5, fatigue life at the different stress amplitude was in the order of 10^5 cycles, indicating that the crack propagation played an important role in the fatigue process.

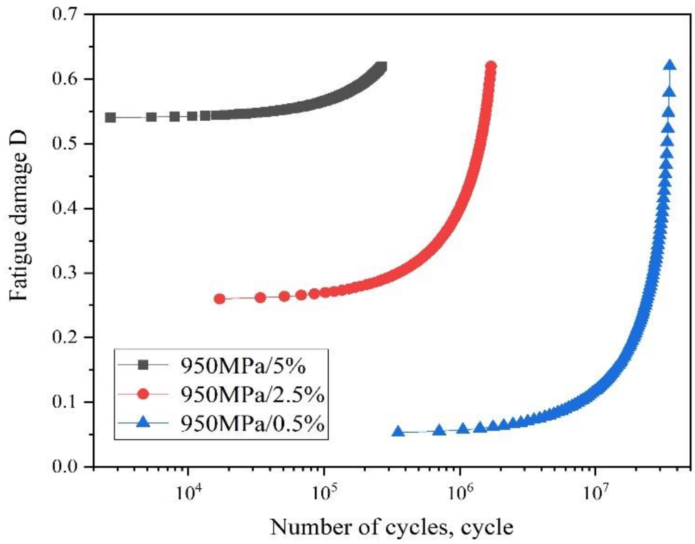

Figure 9. Prediction of fatigue damage evolution for different LCF predamage specimens at 450 MPa stress amplitude.

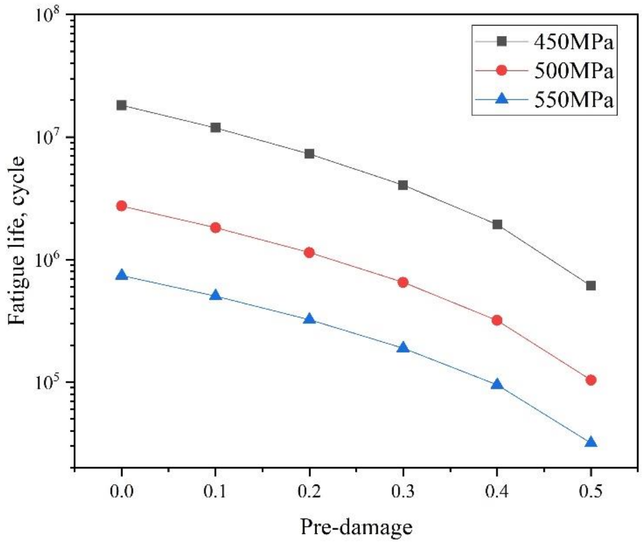

Figure 10. Effect of predamage on fatigue life at different stress amplitude.

To reveal the crack initiation and propagation process for LCF predamage specimens, crack growth life N_p can be estimated as [9]:

$$N_{\rm p} = \frac{(a_{fr}^{1-m/2} - a_0^{1-m/2})}{[1-(m/2)]C(0.65\Delta\sigma\sqrt{\pi})^m} \tag{20}$$

where a_0 and a_{fr} were the size of VHCF critical crack growth and fatigue fracture, respectively, which can be estimated by Formulas (16) and (17). For fatigue crack growth of TC21 titanium alloy, the parameters c and m were determined as 8.64×10^{-13} and 5.066, respectively [9].

Combined with Formulas (19) and (20), the crack initiation life ratio of different LCF predamage at different stress amplitude is shown in Figure 11. The fatigue crack initiation life ratio of specimens with 5% predamage decreased significantly with the increase in stress amplitude. Fatigue crack initiation life ratio at 450 MPa stress amplitude took up 55% of the total life, and decreased to about 15% at 540 MPa stress amplitude where fatigue crack growth life contributed to the main life. It was inferred that the crack growth of TC21 titanium alloy with LCF predamage larger than 5% accounted for the main fatigue damage, which was consistent with the previous investigation [9].

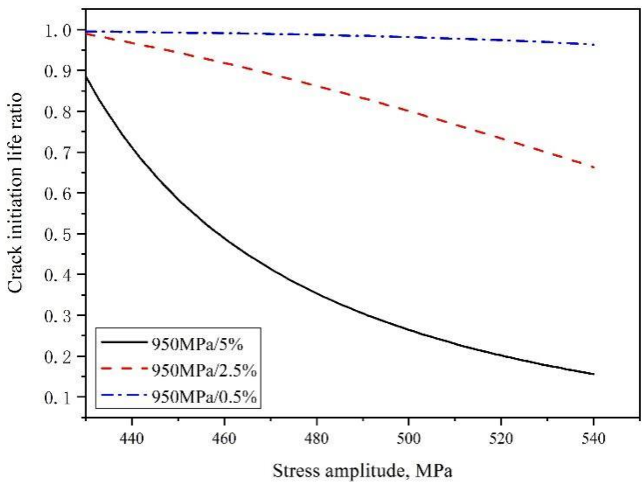

Figure 11. Prediction of fatigue crack initiation life ratio of TC21 titanium alloy after LCF predamage.

However, the fatigue crack initiation of the specimens with LCF predamage less than 5% still took up the major components. Overall, 0.5% predamage had little influence on the subsequent fatigue crack initiation life ratio. As for 2.5% predamage, crack initiation life ratio decreased with the increase of stress amplitude, the fatigue crack initiation life ration was 94% of the total life at 450 MPa stress amplitude, and the proportion of fatigue crack initiation reached about 65% at 540 MPa stress amplitude.

4. Conclusions

1. LCF predamage with less than 5% of fatigue life had little influence on fatigue limit of TC21 titanium alloy, but reduced fatigue life. Fatigue cracks initiated on the surface of the specimen at high stress amplitude, while fatigue cracks initiated on the subsurface of the specimens at low stress amplitude, and crack initiation site presented the bright particle characteristics.
2. Based on Lemaitre damage theory, a very high/low cycle combined fatigue damage model was established to analyze the fatigue damage process, which was consistent with the experimental data. The 5% LCF pre-damage value was the equivalent damage value which was close to the critical value of VHCF crack initiation. Fatigue crack initiation of the specimens with LCF predamage less than 5% took up the major components.

Author Contributions: Z.Z. and D.C. conceived and designed the research; S.L., Y.W., Y.S., H.Q. and B.S. performed the experiment; B.N. analyzed and wrote the manuscript. All authors have read and agreed to the published version of the manuscript.

Funding: This research was funded by R and D plan for key areas in Guangdong Province (2020B01018 6001), Core technology research project of Foshan (1920001000412), Basic and applied basic research fund project in Guangdong Province (2020b15120093), Science and technology project in Guangdong (2020B121202002), R and D plan for key areas in Jiangxi Province (20201BBE51009, 20212BBE51012), Foshan Material Computing Engineering Technology Research Center, Innovation driven project of science and technology plan in Jiangxi Yichun and Graduate Free Exploration Fund of Foshan University (2021ZYTS10).

Data Availability Statement: Not applicable.

Conflicts of Interest: The authors declare no conflict of interest.

References

1. Zhao, Q.; Sun, Q.; Xin, S.; Chen, Y.; Wu, C.; Wang, H.; Xu, J.; Wan, M.; Zeng, W.; Zhao, Y. High-strength titanium alloys for aerospace engineering applications: A review on melting-forging process. *Mater. Sci. Eng. A* **2022**, *845*, 143260. [CrossRef]
2. Gao, T.; Xue, H.; Sun, Z.; Retraint, D.; He, Y. Micromechanisms of crack initiation of a Ti-8Al-1Mo-1V alloy in the very high cycle fatigue regime. *Int. J. Fatigue* **2021**, *150*, 106314. [CrossRef]
3. Gao, T.; Xue, H.; Sun, Z.; Retraint, D. Investigation of crack initiation mechanism of a precipitation hardened TC11 titanium alloy at very high cycle fatigue loading. *Mater. Sci. Eng. A* **2020**, *776*, 138989. [CrossRef]
4. Liu, F.; Peng, H.; Liu, Y.; Wang, C.; Wang, Q.; Chen, Y. Crack initiation mechanism of titanium alloy in very high cycle fatigue regime at 400 °C considering stress ratio effect. *Int. J. Fatigue* **2022**, *163*, 107012. [CrossRef]
5. Li, C.; Li, W.; Cai, L.; Zhang, Y.; Sun, R.; Li, X.; Wang, P. Microstructure based cracking behavior and life assessment of titanium alloy at very-high-cycle fatigue with elevated temperatures. *Int. J. Fatigue* **2022**, *161*, 106914. [CrossRef]
6. Liu, F.; Chen, Y.; He, C.; Li, L.; Wang, C.; Li, H.; Liu, Y. Tensile and very high cycle fatigue behaviors of a compressor blade titanium alloy at room and high temperatures. *Mater. Sci. Eng. A* **2021**, *811*, 141049. [CrossRef]
7. Huang, Z.Y.; Wanger, D.; Bathias, C.; Chaboche, J.L. Cumulative fatigue damage in low cycle fatigue and gigacycle fatigue for low carbon-manganese steel. *Int. J. Fatigue* **2011**, *33*, 115–123. [CrossRef]
8. Huang, Z.Y.; Wang, Q.Y.; Wagner, D.; Bathias, C. Effect of low cycle fatigue predamage on very high cycle fatigue. *Theor. Appl. Mech. Lett.* **2012**, *2*, 031007. [CrossRef]
9. Nie, B.; Zhao, Z.; Ouyang, Y.; Chen, D.; Chen, H.; Sun, H.; Liu, S. Effect of low cycle fatigue predamage on very high cycle fatigue behavior of TC21 titanium alloy. *Materials* **2017**, *10*, 1384. [CrossRef]
10. Pavlou, D. The theory of the S-N fatigue damage envelope: Generalization of linear, double-linear, and non-linear fatigue damage models. *Int. J. Fatigue* **2018**, *110*, 204–214. [CrossRef]

11. Qiu, S.; Cui, H.; Zhang, H.; Wen, W.; Guo, J. A dual-threshold modelling approach for fatigue life prediction at combined high and low cycle fatigue. *Int. J. Fatigue* **2022**, *164*, 107110. [CrossRef]
12. Yue, P.; Ma, J.; Huang, H.; Shi, Y.; Zu, J. Threshold damage-based fatigue life prediction of turbine blades at combined high and low cycle fatigue. *Int. J. Fatigue* **2021**, *150*, 106323. [CrossRef]
13. Zhao, Z.; Wang, L.; Liu, L.; Chen, W. Prediction of combined cycle fatigue life of TC11 alloy based on modified nonlinear cumulative damage model. *Chin. J. Aeronaut.* **2021**, *34*, 73–84. [CrossRef]
14. Schweizer, C.; Seifert, T.; Nieweg, B.; Von Hartrott, P.; Riedel, H. Mechanisms and modelling of fatigue crack growth at combined low and high cycle fatigue loading. *Int. J. Fatigue* **2011**, *33*, 194–202. [CrossRef]
15. Morrissey, R.J.; Golden, P.; Nicholas, T. The Effect of Stress Transients on the HCF Endurance Limit in Ti-6Al-4V. *Int. J. Fatigue* **2003**, *25*, 1125–1133. [CrossRef]
16. Hu, D.; Yang, Q.; Liu, H.; Mao, J.; Meng, F.; Wang, Y.; Wang, R. Crack closure effect and crack growth behavior in GH2036 superalloy plates at combined high and low cycle fatigue. *Int. J. Fatigue* **2017**, *95*, 90–103. [CrossRef]
17. Li, X.; Song, L.; Bai, G. Deep learning regression-based stratified probabilistic combined cycle fatigue damage evaluation for turbine bladed disks. *Int. J. Fatigue* **2022**, *159*, 106812. [CrossRef]
18. Bai, S.; Li, Y.; Huang, H.; Ma, Q.; Lu, N. A probabilistic combined high and low cycle fatigue life prediction framework for the turbine shaft with random geometric parameters. *Int. J. Fatigue* **2022**, *165*, 107218. [CrossRef]
19. Gao, H.; Zio, E.; Wang, A.; Bai, G.; Fei, C. Probabilistic-based combined high and low cycle fatigue assessment for turbine blades using a substructure-based kriging surrogate model. *Aerosp. Sci. Technol.* **2020**, *104*, 105957. [CrossRef]
20. Li, G.; Ke, L.; Ren, X.; Sun, C. High cycle and very high cycle fatigue of TC17 titanium alloy: Stress ratio effect and fatigue strength modeling. *Int. J. Fatigue* **2023**, *166*, 107299. [CrossRef]
21. Liu, X.; Wang, X.; Liu, Z.; Chen, Z.; Sun, Q. Continuum damage mechanics based probabilistic fatigue life prediction for metallic material. *J. Mater. Res. Technol.* **2022**, *18*, 75–84. [CrossRef]
22. Lemaitre, J.; Sermage, J.; Desmorat, R. A two scale damage concept applied to fatigue. *Int. J. Fract.* **1999**, *97*, 67–81. [CrossRef]
23. Nie, B.; Liu, S.; Huang, X.; Qi, H.; Shi, B.; Zhao, Z.; Chen, D. Low cycle fatigue crack damage behavior of TC21 titanium alloy with basketweave microstructure. *Crystals* **2022**, *12*, 1211. [CrossRef]
24. Nie, B.; Song, Y.; Huang, X.; Qi, H.; Zhao, Z.; Chen, D. Low Cycle fatigue behavior of TC21 titanium alloy with bi-Lamellar basketweave microstructure. *Crystals* **2022**, *12*, 796. [CrossRef]
25. Bathias, C. Piezoelectric fatigue testing machines and devices. *Int. J. Fatigue* **2006**, *28*, 1438–1445. [CrossRef]
26. Ren, W.; Nicholas, T. Effects and mechanisms of low cycle fatigue and plastic deformation on subsequent high cycle fatigue limit in nickel-base superalloy Udimet 720. *Mater. Sci. Eng. A* **2002**, *332*, 236–248. [CrossRef]
27. Lemaitre, J.; Desmorat, R. *Engineering Damage Mechanics: Ductile, Creep, Fatigue and Brittle Failures*; Springer: Dordrecht, The Netherlands, 2006.
28. Krewerth, D.; Lippmann, T.; Biermann, H. Influence of non-metallic inclusions on fatigue life in the very high cycle fatigue regime. *Int. J. Fatigue* **2016**, *84*, 40–52. [CrossRef]